doi:10.1016/j.jmb.2011.01.044 J. Mol. Biol. (2011) 407, 465–476

Contents lists available at www.sciencedirect.com

Journal of Molecular Biology

journal homepage: http://ees.elsevier.com.jmb

Effects of the Known Pathogenic Mutations on the Aggregation Pathway of the Amyloidogenic Peptide of Apolipoprotein A-I

Sara Raimondi[1,2]†, Fulvio Guglielmi[3]†, Sofia Giorgetti[1], Sonia Di Gaetano[4], Angela Arciello[3], Daria M. Monti[3], Annalisa Relini[5,6], Daniela Nichino[5], Silvia M. Doglia[7], Antonino Natalello[7], Piero Pucci[6,8], Palma Mangione[1], Laura Obici[2], Giampaolo Merlini[1,2], Monica Stoppini[1,6], Paul Robustelli[9], Gian Gaetano Tartaglia[10], Michele Vendruscolo[9], Christopher M. Dobson[9], Renata Piccoli[3,6] and Vittorio Bellotti[1,2,6]*

[1]*Department of Biochemistry, University of Pavia, 27100 Pavia, Italy*
[2]*Biotechnology Laboratories, IRCCS Policlinico San Matteo, 27100 Pavia, Italy*
[3]*Department of Structural and Functional Biology, School of Biotechnological Sciences, University of Naples Federico II, 80126 Naples, Italy*
[4]*Institute of Biostructures and Bioimages, CNR, 80134 Naples, Italy*
[5]*Department of Physics, University of Genoa, 16146 Genoa, Italy*
[6]*Istituto Nazionale di Biostrutture e Biosistemi (INBB), 00136 Rome, Italy*
[7]*Department of Biotechnology and Biosciences, University of Milano-Bicocca, 20126 Milan, Italy*
[8]*Department of Organic Chemistry and Biochemistry, University of Naples Federico II and Ceinge Biotecnologie Avanzate, 80145 Naples, Italy*
[9]*Department of Chemistry, University of Cambridge, Cambridge CB2 1EW, UK*
[10]*CRG Centre for Genomic Regulation, Dr Aiguader 88, Barcelona 8003, Spain*

Received 12 August 2010; received in revised form 22 December 2010; accepted 23 January 2011
Available online 4 February 2011

Edited by S. Radford

Keywords:
structural transitions; amyloidogenic mutations; apolipoprotein A-I; proteolytic cleavage; fibrillogenesis

The 93-residue N-terminal fragment of apolipoprotein A-I (ApoA-I) is the major constituent of fibrils isolated from patients affected by the amyloidosis caused by ApoA-I mutations. We have prepared eight polypeptides corresponding to all the currently known amyloidogenic variants of the N-terminal region of ApoA-I, other than a truncation mutation, and investigated their aggregation kinetics and the associated structural modifications. All the variants adopted a monomeric highly disordered structure in solution at neutral pH, whereas acidification of the solution induced an unstable α-helical conformation and the subsequent aggregation into the cross-β structure aggregate. Two mutations (Δ70–72 and L90P) almost abrogated the lag phase of the aggregation process, three mutations (Δ60–71, L75P, and W50R) significantly accelerated the aggregation rate by 2- to 3-fold, while the remaining three variants (L64P, L60R, and G26R) were not significantly different from the wild type. Therefore, an increase in aggregation propensity cannot explain *per se* the

**Corresponding author*. Department of Biochemistry, University of Pavia, via Taramelli 3b, 27100 Pavia, Italy. E-mail address: vbellot@unipv.it.

† S.R. and F.G. contributed equally to this work.

Abbreviations used: ApoA-I, apolipoprotein A-I; [1–93]ApoA-I, 1–93 region of apolipoprotein A-I; GST, glutathione *S*-transferase; AFM, atomic force microscopy; CD, circular dichroism; FTIR, Fourier transform infrared spectroscopy; ATR, attenuated total reflection; MS, mass spectrometry.

mechanism of the disease for all the variants. Prediction of the protection factors for hydrogen exchange in the native state of full-length protein reveals, in almost all the variants, an expansion of the conformational fluctuations that could favour the proteolytic cleavage and the release of the amyloidogenic peptide. Such an event seems to be a necessary prerequisite for ApoA-I fibrillogenesis *in vivo*, but the observed increased aggregation propensity of certain variants can have a strong influence on the severity of the disease, such as an earlier onset and a faster progression.

Introduction

Apolipoprotein A-I (ApoA-I), the primary protein component of high-density lipoproteins, plays a crucial role in the removal of cholesterol from cells.[1] A variety of mutations in the ApoA-I gene have been associated with familial hypercholesterolemia,[2] a prototypic "loss-of-function" genetic disease, while other mutations have been associated with familial systemic amyloidosis, which represents a genetic disease prototypically characterized by a gain of a pathological function.[3] In addition, the soluble form of wild-type human ApoA-I can give rise to amyloid deposits into atheromasic plaques, although their pathogenic role is currently uncertain.[4] An extensive proteomic analysis (reviewed in Ref. 3) of natural amyloid fibrils has demonstrated that, although traces of full-length ApoA-I are detectable in disease-associated fibrils, their main components are heterogeneous N-terminal fragments of the protein, with the 1–93 peptide (denoted here as [1–93]ApoA-I) being the most abundant and persistent species among all the specimens investigated thus far.

Analysis of the mutations in ApoA-I associated with the disease showed that they can be located either within or outside the 1–93 region of the sequence. It has been suggested,[3] however, that "outside mutations" might favour the release of the intrinsically amyloidogenic [1–93]ApoA-I fragment, while "inside mutations" would directly enhance the aggregation propensity of the natively unfolded [1–93]ApoA-I fragment upon its release from the full-length protein. Thus far, nine amyloidogenic ApoA-I variants carrying "inside mutations" have been identified,[3,5] but the effects of these mutations on the kinetics of aggregation of [1–93]ApoA-I have not yet been investigated, primarily because of difficulties in the production of the recombinant form of the peptide. However, recently we have produced a recombinant version of [1–93]ApoA-I, providing us with an opportunity to carry out such experiments. In the present paper, we have studied the aggregation propensity of eight pathogenic isoforms of [1–93]ApoA-I, which represent all the amyloidogenic "inside mutations" associated with ApoA-I currently identified,[3] with the exception of the frameshift mutation (Asn74fs) recently reported by Eriksson *et al.*[5] For these isoforms, we have investigated the structural transitions induced by lowering the pH, along with the kinetics of aggregation and the structural properties of the aggregated material. Comparison of these experimental data with sequence-based predictions of the aggregation propensities[6] and stabilities[7] supports the hypothesis that the amyloidogenic mutations of ApoA-I enhance the flexibility of the region of the protein spanning approximately residues 88–110, thus facilitating the release of the N-terminal amyloidogenic peptide;[8] however, certain mutations can further boost the process of amyloid formation by conferring to the peptide a higher aggregation propensity.

Results

The present study is focused on a comparative analysis of the aggregation propensities of a series of mutational variants of [1–93]ApoA-I, which includes all the "inside mutations" of ApoA-I previously described, other than one frameshift variant.[3,5] Mutated cDNA constructs were obtained by site-directed mutagenesis for the six variants (G26R, W50R, L60R, L64P, L75P, and L90P) with a single residue substitution. The other two variants contain sequence deletions at positions 70–72 (Δ70–72) or at positions 60–71; in the latter case, the deleted residues are replaced by Val and Thr residues, respectively (Δ60–71/VT). We have generated the eight mutated isoforms of [1–93]ApoA-I (Supplementary Fig. S1) using the same experimental strategy successfully applied to produce the recombinant form of wild-type [1–93] ApoA-I.[9] Briefly, since the natural peptide is natively unfolded, its variants were expressed in bacterial cells as chimeric proteins, in which the 93-residue peptide is fused to glutathione *S*-transferase (GST) to enhance its stability and protect it from proteolysis.

All the recombinant peptide variants were analysed by electrospray mass spectrometry (MS) in order to confirm their homogeneity and their correct amino acid sequence. A small aliquot of each sample was desalted by HPLC and injected directly in the

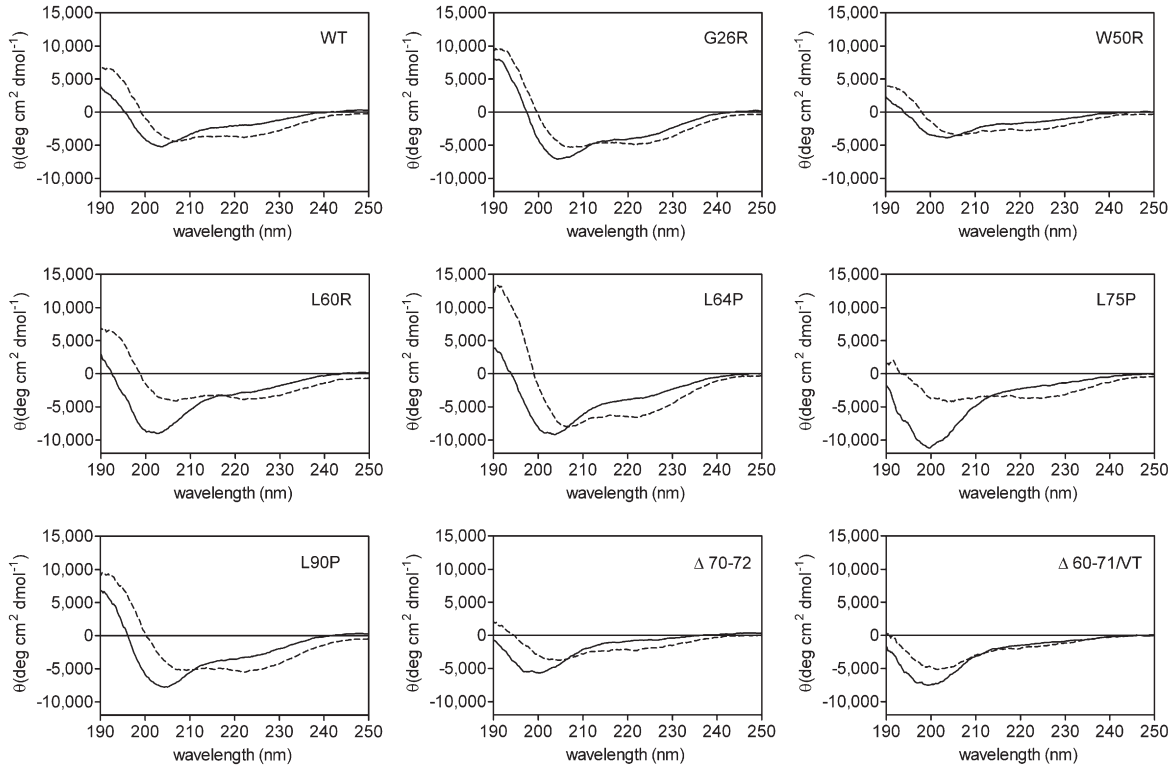

Fig. 1. Far-UV CD spectra of the [1–93]ApoA-I variants. CD spectra were recorded at pH 7.0 (—▲—) and pH 4.0 (—○—). WT, wild type.

electrospray MS source. The sample corresponding to wild-type [1–93]ApoA-I gave rise to a single peak corresponding to a molecular mass of 10,863.4 ± 0.3 Da, in excellent agreement with the expected mass value of the [1–93]ApoA-I peptide carrying at the N-terminus the Gly-Ser extra dipeptide associated with the thrombin cleavage strategy.[9] Mass spectral analysis of all the [1–93]ApoA-I mutants confirmed in each case the expected amino acid substitution (Supplementary Table S1). In addition to the expected species, all the variants showed the presence of a minor component (ranging from 8% to 47%) with a mass 16 Da higher than the parent peptides, deriving from Met oxidation (Supplementary Table S1). Before using this material for further analyses, we checked whether Met oxidation might affect peptide behaviour. The native 1–93 peptide purified from natural fibrils (not oxidised) and the recombinant peptide (containing the oxidised form) were compared and found to give identical circular dichroism (CD) spectra at pH 7 and pH 4 as well as identical kinetics of aggregation (data not shown). Furthermore, we did not detect any correlation between the percentage of oxidised species of individual peptides and the aggregation propensity of the species itself (see below). In addition, to exclude an effect of oxidation, we have carried out the aggregation of two representative species of [1–93]ApoA-I peptide (wild-type and L75P) by comparing the nonoxidised and fully oxidised forms, respectively. Data reported in Supplementary Fig. S4 demonstrate that the oxidation does not modify the aggregation kinetics.

Before further investigations, the oligomeric state of the amyloidogenic [1–93]ApoA-I fragment was assessed by gel-filtration chromatography. The recorded elution volume was consistent with a monomeric form of a natively unfolded protein with an elongated shape. This result was further confirmed by sedimentation equilibrium experiments from which a molecular mass of 10,427 ± 957 Da was estimated (Supplementary Fig. S5). Altogether, these data demonstrated that [1–93]ApoA-I did not form aggregates in these conditions.

For all the recombinant variants studied here, we monitored the changes in structure induced by the reduction of pH, along with the kinetics of aggregation and the acquisition of the cross-β structure in the aggregated material. All the [1–93]ApoA-I displayed CD spectra consistent with a highly disordered conformation (Fig. 1). Acidification of the buffer to pH 4, however, resulted in an increase of the helical structure (Fig. 1); the Δ70–72 and Δ60–71/VT variants showed the lowest increase in α-helical content (8% and 2%, respectively;

Table 1. Estimation of the α-helix contents and aggregation propensities of the eight [1–93]ApoA-I variants under investigation

	pH 7	pH 4	Increase in		Zagg + CamP[b]
	α-Helix (%)	α-Helix (%)	α-helix (%)	k_{AGG}[a]	score
Wild-type	15	29	14	1.6 ± 0.3	0.46 ± 0.02
G26R	25	43	18	2.3 ± 0.5	0.47 ± 0.02
W50R	8	26	18	4.4 ± 0.7	0.64 ± 0.02
L60R	11	29	18	2.1 ± 0.4	0.48 ± 0.02
L64P	13	57	44	1.4 ± 0.3	0.46 ± 0.02
L75P	9	25	16	3.7 ± 0.7	0.52 ± 0.02
L90P	13	48	35	n.d.[c]	0.79 ± 0.02
Δ60–71/VT	9	11	2	2.7 ± 0.5	0.48 ± 0.02
Δ70–72	9	17	8	n.d.[c]	0.66 ± 0.02

Percentages of α-helical structure were determined from the far-UV CD spectra of the proteins at pH 7 and pH 4, respectively, and the relative increase in helical content, upon acidification, is reported. The K2D2 web server[10] was used for the evaluation of the secondary-structure content.

[a] Aggregation rate constants (10^{-4} s^{-1}) determined using spectrophotometrical data at 350 nm; mean ± SD from three independent measurement.

[b] Zagg aggregation propensities calculated using the Zyaggregator method at pH 4.[6] The conformational fluctuations are predicted using the CamP method.[7]

[c] These variants were already partially aggregated at time zero.

Table 1); for the other variants, the increase of the secondary structure varied from 14% to 44%, with L64P and L90P showing the most remarkable changes (Table 1).

All the peptides were found to aggregate at pH 4, as demonstrated by the increase in turbidity monitored at 350 nm (Fig. 2). The rate constants obtained by fitting the data points to single exponential functions are reported in Table 1 for all the variants. L90P and Δ70–72 aggregation occurred in the lag phase of measurement (≤60 s); therefore, their rate constants could not be determined under those conditions. Δ60–71/VT, L75P, and W50R aggregation rates were significantly different from that of the wild type (*P* value <0.05), resulting in a 2- to 3-fold increase. The

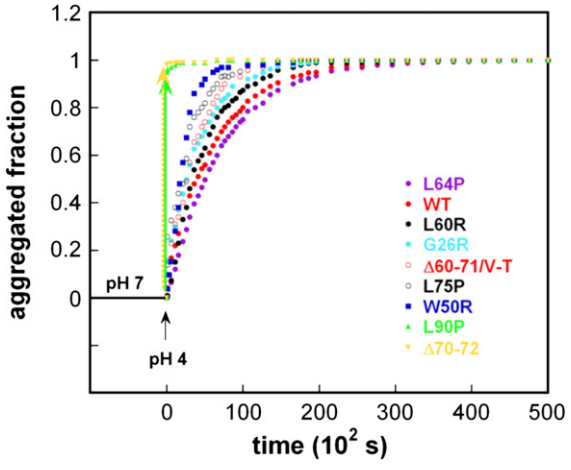

Fig. 2. Aggregation of the [1–93]ApoA-I variants at pH 4.0. Aggregation was monitored before and after acidification of protein solutions from pH 7 to pH 4. The increase in turbidity was monitored spectrophotometrically at 350 nm.

L64P, L60R, and G26R mutations did not produce a significant change in the rate of aggregation compared to the wild-type peptide. In order to explore the structural transitions associated with the aggregation process, the aggregates were analysed by Fourier transform infrared (FTIR) spectroscopy (Fig. 3) after 48 h of incubation at pH 4. The spectra display three major components at ~1695 cm^{-1}, ~1655 cm^{-1}, and ~1622 cm^{-1}, with relative intensities varying for the different variants. The 1695 cm^{-1} and 1622 cm^{-1} components can be assigned to the intermolecular β-sheet structure characteristic of protein aggregates,[11,12] in agreement with what was already reported for the wild-type [1–93]ApoA-I peptide.[13] The component at 1655 cm^{-1} occurs in the absorption region typical of α-helical and random-coil secondary structures.[14] The β-sheet band at 1622 cm^{-1} is clearly evident in the absorption spectra of the G26R, L60R, L64P, L90P, and Δ70–72 variants, as well as in the spectrum of the wild-type peptide, while this band appears as a shoulder in the spectra of the L75P and W50R variants (Fig. 3a). In the latter two cases, we examined the second-derivative spectra to better reveal the β-sheet band (Fig. 3b).[14] The second-derivative spectrum of the G26R variant is also reported for comparison. To evaluate the percentage of intermolecular β-sheet structures in the different aggregates, we performed a Gaussian curve fitting of the measured spectra in the amide I region (Supplementary Fig. S6). The percentage of intermolecular β-sheet structures ranges from 30% to 40% in the wild type and in all the variants, with the exception of L75P and W50R, which display a lower percentage (around ~20%). We can therefore conclude that the aggregates of all the variants display the typical infrared signature of intermolecular β-sheet structures.

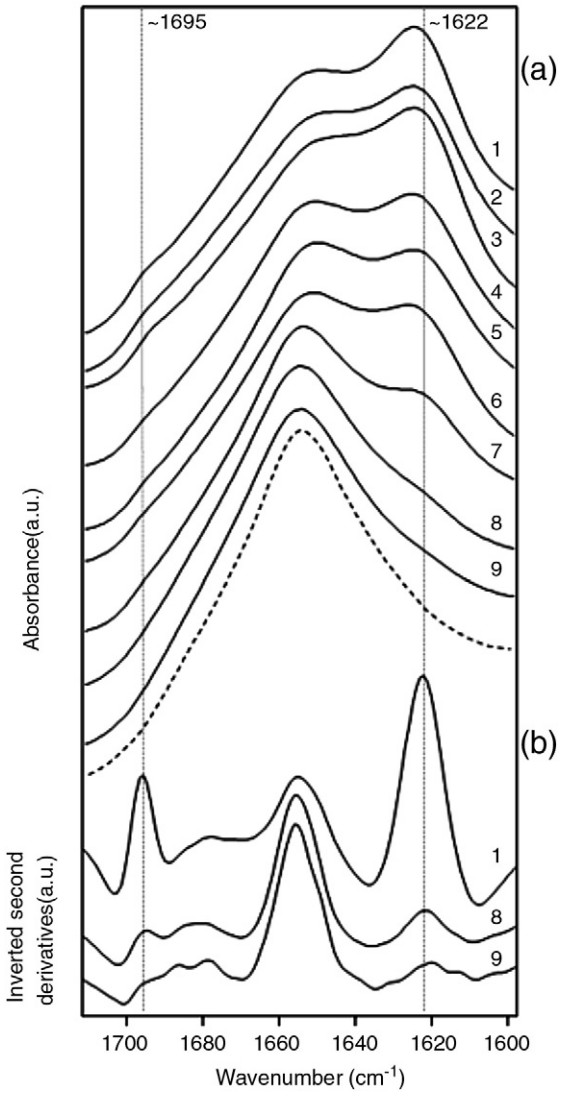

Fig. 3. FTIR spectra of the [1–93]ApoA-I variant aggregates. The aggregates were obtained after incubation of the [1–93]ApoA-I variants at pH 4 for 48 h. (a) ATR/FTIR absorption spectra of G26R (1), L60R (2), Δ60–71/VT (3), L64P (4), wild-type (5), L90P (6), Δ70–72 (7), L75P (8), and W50R (9) at pH 4. The spectrum of wild-type [1–93]ApoA-I at pH 7 (dotted line) is also reported for comparison. (b) Second-derivative spectra of G26R (1), L75P (8), and W50R (9). The evaluation of the intermolecular β-sheet content of the different aggregates is presented in Supplementary Fig. S6.

Tapping-mode atomic force microscopy (AFM) was then used to obtain information about the morphology of the aggregates formed by the series of amyloidogenic [1–93]ApoA-I variants after 48 h of incubation at pH 4. Representative morphologies are shown in Fig. 4. Spheroidal structures of height from 1 to 3 nm were found in all the samples examined. Aggregate sizes were obtained from the height in cross-section of the topographic AFM images; the values here reported are reduced with respect to fully hydrated conditions as a consequence of sample dehydration. These aggregates often tend to form clusters; such behaviour is particularly evident in L75P and Δ70–72 samples (Fig. 4g and h). Very thin filaments of height less than 1 nm are also present in W50R and Δ60–71/VT samples (Fig. 4f and i); in the latter, they are often arranged in networks and coexist with nonfibrillar material (Fig. 4i).

These aggregates are not positive to the thioflavin staining and have not the features of the amyloid fibrils that become clearly visible after 2 weeks of incubation. These data suggest that the events leading to fibril formation, such as the acquisition of the β structure, take place in the early stage of aggregation, but a progressive and slow rearrangement of the aggregate is required to form classic amyloid fibrils. It is worth of note that amyloid fibrils *in vivo* are associated with prominent protein deposits of the ApoA-I peptide; such deposits are lacking the typical fibrillar features at the electron microscope and are then described as an amorphous aggregate.[15]

Experimental data concerning the aggregation propensities of wild-type [1–93]ApoA-I and its eight variants were compared with theoretical predictions obtained by the Zyggregator method,[6] which is based on the analysis of the physicochemical properties of the amino acid sequences, such as hydrophobicity and electrostatic charge, which are important in determining their aggregation behaviour (Table 1 and Fig. 5a). The peaks in the aggregation propensity profile of full-length ApoA-I indicate that residues 15–20 and 50–57 are the most aggregation-prone regions at pH 4. The predicted values of the aggregation propensity of the variants are in good agreement with those experimentally determined, and a linear correlation coefficient and a probability value of 0.89 and 0.007, respectively, were obtained (Fig. 5b).

In order to characterise the process by which the naturally occurring pathogenic mutations of [1–93]ApoA-I peptide favour its proteolytic release, we carried out predictions of the changes that these mutations induce in the polypeptide conformational fluctuations. In order to estimate such changes, we used the CamP method,[7] by which the flexibility and the solvent accessibility of proteins are predicted with high accuracy. This method enables the prediction from the amino acid sequence of the buried regions with more than 80% accuracy and of the protection factors by hydrogen exchange with an average accuracy of 60%. The predicted protection factor of the variants is consistently lower than that of the wild-type, ranging from the minimal differences observed for the L64P variant to the largest changes observed for Δ60–71/VT. These results suggest that the mutations might enhance the

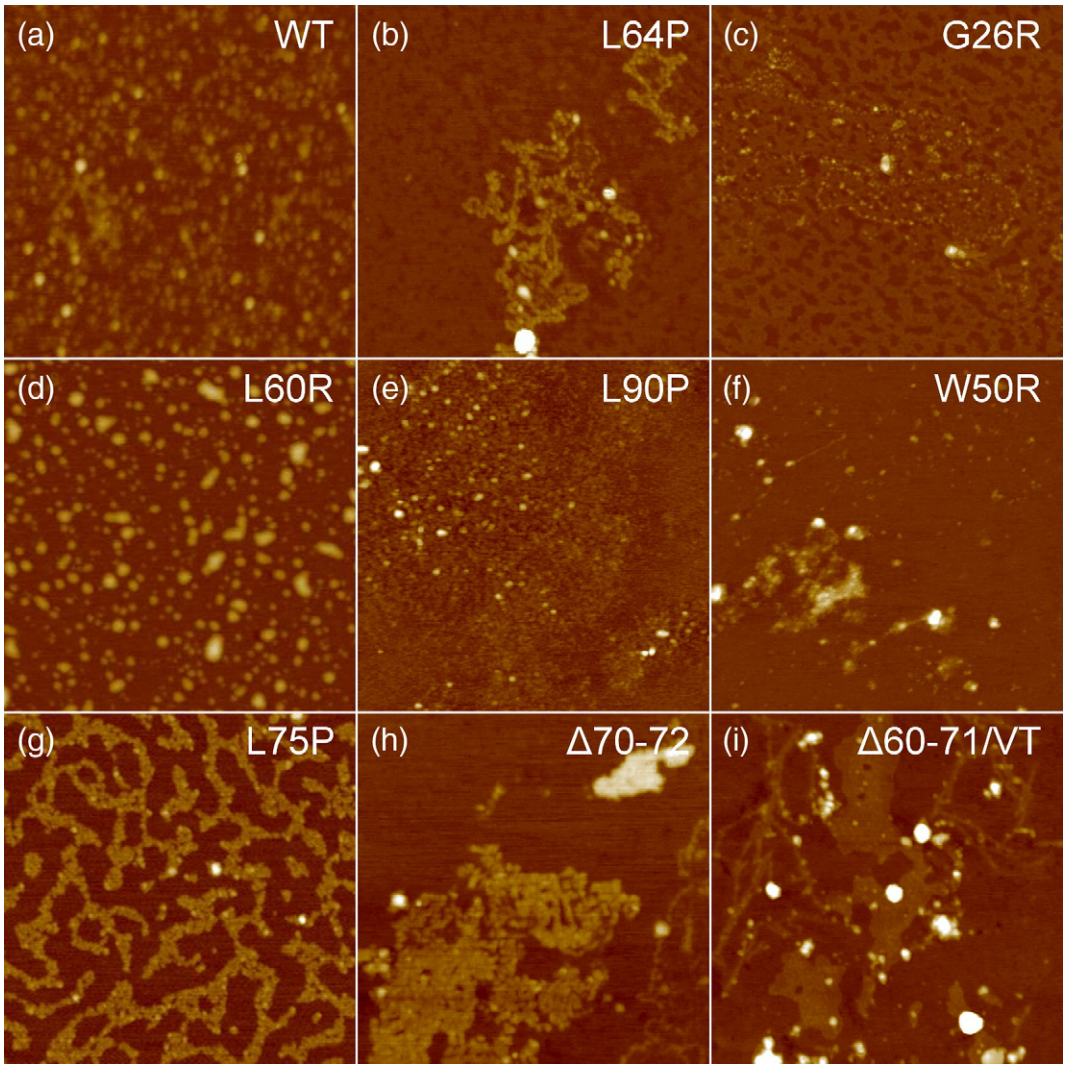

Fig. 4. Tapping-mode AFM images (height data) showing typical morphologies of the aggregates formed by the [1–93] ApoA-I mutants after 48 h incubation at pH 4. Scan size, 1 μm. Z range: 15 nm (a, d, i); 10 nm (b, e, f, h); 8 nm (c); 5 nm (g).

conformational fluctuations and chain flexibility in the proximity of the putative cleavage site (Fig. 6), displaying a general trend of reduced protection for all the amyloidogenic variants.

Discussion

We have previously shown that [1–93]ApoA-I can be promptly converted into amyloid fibrils upon lowering the pH from 7 to 4.[9,13] However, the roles of the amyloidogenic mutations located inside this peptide and their effects on the kinetics of aggregation were not elucidated yet. In this study, the availability of the [1–93]ApoA-I variants, representative of eight natural amyloidogenic species, has provided the unique opportunity of investigating their role in promoting protein aggregation. We have found that two mutations (Δ70–72 and L90P) remarkably accelerate the aggregation kinetics of [1–93]ApoA-I; in fact, the aggregation of these two variants is very fast and fully accomplished in the lag phase of the measurement. Also, the Δ60–71, L75P, and W50R mutations produce a statistically significant change (P value <0.05) in the rate of aggregation, producing a 2- to 3-fold increase. No statistically significant difference can be detected in the presence of all the remaining mutations whose aggregation rates overlap that of the wild-type species. It is worth of note that the experimentally determined values of the aggregation rate well correlate with the predicted aggregation propensity obtained through the Zyggregator algorithm at pH 4 (Fig. 5b).[6]

The insoluble material was recovered after 48 h, at the end of the aggregation phase, and displayed the

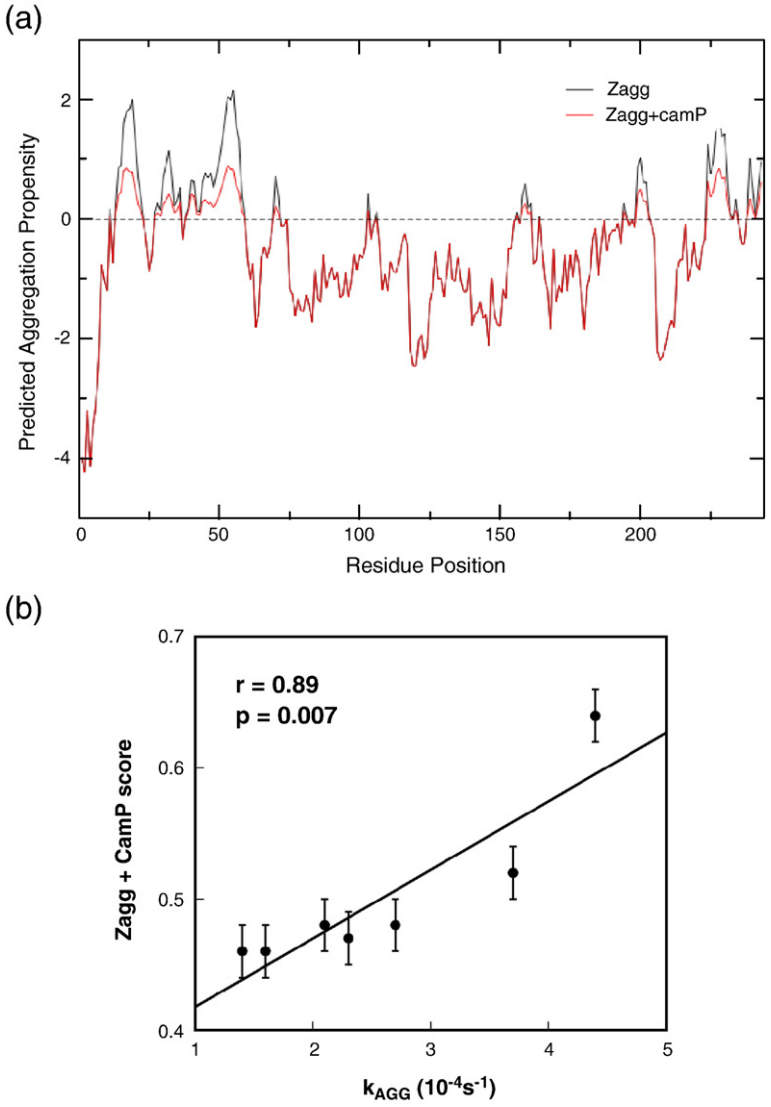

Fig. 5. (a) Zagg aggregation propensities of ApoA-I calculated with the Zyggregator method at pH 4. Zagg represents the intrinsic propensity to form amyloid aggregates calculated from the unfolded state (black line). Zagg + CamP or "structural correction" estimates the propensity to form amyloid aggregates in a near-native state (red line).[6] It works as a correction for the intrinsic propensity to form amyloid aggregates. Residues 15–20 and 50–57, which are included in the N-terminal portion of the protein, are the most aggregation prone. (b) Linear correlation between experimental aggregation rate and aggregation propensity calculated using the Zyggregator method at pH 4.

spectroscopic features (Fig. 3) of intermolecular β-sheet structures typical of amyloid aggregate. However, the AFM analysis of the aggregates shows the presence of spheroidal structures, often assembled into clusters and filaments, but not mature fibrils that become visible in the specimens only after 72 h of incubation (data not shown).

The conformational changes occurring along the aggregation are similar for all the [1-93]ApoA-I variants and indicate the transient acquisition of an α-helical secondary structure in six of the eight variants. It is worthy of note that in the two cases involving deletion and deletion/insertion mutations, the α-helical secondary structure is minimal and both species have a strong tendency to aggregate. This finding suggests that the acquisition of a transient α-helical structure is not a pre-requisite for the β-aggregation, but it might represent an alternative conformation that, if stabilised by natural ligands such as phospholipids[13] or cholesterol,[16] can prevent the peptide aggregation.

The evidence that, in comparison with the wild-type species, three of the eight variants do not display a faster aggregation rate suggests that an increased aggregation propensity linked to the mutations cannot fully explain *per se* the molecular basis of this hereditary amyloidosis, but an additional mechanism is required.

Proteomic studies carried out on natural fibrils[8] highlight that cleavage points are all clustered between residues 83 and 96, whereas the "internal" mutations are located between residues 26 and 93. The region including residues 83–96 should constitute a loop interconnecting two helical bundles according to Lagerstedt *et al.*,[17] who compared the secondary structure determined by electron paramagnetic resonance spectroscopy with the available 3D structure of ApoA-I (PDB 2A01).[18] Although the

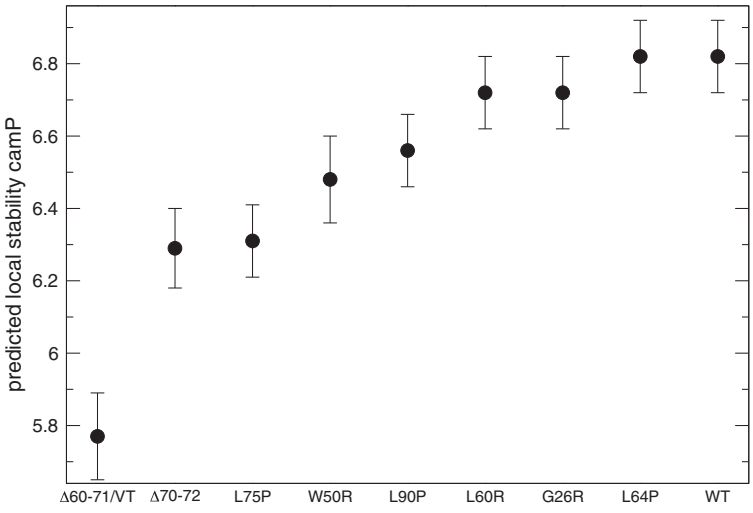

Fig. 6. Protection factors of the eight amyloidogenic variants studied in this work calculated using the CamP method.[7] These results illustrate the increase in the structural fluctuations upon mutation that is associated with the protection factor reduction.

latter is currently under dispute as reported in a PNAS editorial expression of concern‡, the conformation of the region spanning residues 83–96 is similar in the structures reported by Ajees *et al.*[18] and Lagerstedt *et al.*[17] The loop could represent a flexible region accessible to proteases, and the amyloidogenic mutations might enhance side-chain mobility in the region 83–96, thus permitting proteolytic cleavage and the release of the amyloidogenic N-terminal segment of the molecule. This observation is in agreement with the findings of Lagerstedt *et al.*[19] reporting that the G26R mutation destabilises the protein, thus providing an indirect experimental support to the hypothesis that the pathologic protein becomes more susceptible to the proteases-mediated release of the N-terminal amyloidogenic domain. Our prediction that the effect of the mutations affects the conformational flexibility of the ApoA-I chain, in the proximity of the site of the cleavage, is therefore fully consistent with the hypothesis of Lagerstedt *et al.*[19]

Analysis of *ex vivo* amyloid fibrils of patients carrying some of the "inside mutations" (L60R, Δ60–71/VT, and W50R) clearly showed that fibrils are preferentially constituted by the mutated peptides.[20–23] It is therefore likely that the susceptibility to the proteolytic cleavage is only limited to the polypeptide carrying the mutation and does not influence the processing of the normal counterpart that, in the high-density lipoprotein complex, is expected to be assembled with the variant.

It is therefore highly plausible that certain mutations might cause both an increased shedding of the amyloidogenic peptide as well as a faster aggregation rate, thus influencing the clinical history of the disease through a synergic combination of the two mechanisms. It is worthy to note that the two mutations displaying the fastest (Δ70–72) and the slowest (L64P) aggregation rates were both identified in patients affected by renal amyloidosis, but were respectively associated with the earliest (II decade)[24] and latest (VI decade)[25] age of onset of the failure of the target organ. This observation suggests that a possible correlation might exist between the aggregation propensity of the variant and an earlier onset of the disease. However, at this stage, this correlation cannot be easily extended to other cases because, in several cases, the disease onset is not always precisely reported in the clinical reports.

‡ http://www.pnas.org/content/107/14/6551.3.full?sid=daacdccb-0537-41fb-87c3-8%2067aba380ca7

Materials and Methods

Construction and expression of [1–93]ApoA-I variants

Site-directed mutagenesis of the cDNA encoding [1–93] ApoA-I was performed by PCR amplification (Applied Biosystems, Foster City, CA) using pairs of oligonucleotides carrying the desired mutation. Restriction sites were positioned at the 5′-end of the primers (BamHI in forward primers, EcoRI in reverse primers). With the exception of variant L90P, mutated cDNAs were obtained by overlap extension PCR mutagenesis.[26] PCR products were purified using a DNA purification system (Promega Biosciences Inc., San Luis Obispo, CA), digested with BamHI and EcoRI enzymes, and cloned into the corresponding sites of the pGEX-4T-3 expression vector, downstream of the sequence encoding GST. The expression vector had previously been digested with the same enzymes and treated with shrimp alkaline phosphatase (Roche Applied Science, Indianapolis, IN). The recombinant products were fully sequenced by Eurofins-MWG (Ebersberg, Germany). [1–93]ApoA-I variants were expressed as GST-fused proteins as described previously for the wild-type polypeptide.[9] Briefly, the GST-fused proteins were isolated by affinity chromatography on a GSTrap

glutathione–agarose column (GE Healthcare, Piscataway, NJ). Following site-directed proteolysis, ApoA-I polypeptides were purified by HPLC reverse chromatography on a C-8 column (Ultrapure C-8, Grace Vydak, Deerfield, IL). A gradient of buffer B (acetonitrile containing 0.1% TFA) in buffer A (0.1% TFA in water) was achieved at a flow rate of 1 ml/min, using the Perkin Elmer Series 200 chromatographic system (00). For each variant of [1–93] ApoA-I, optimal elution conditions were established by varying the elution parameters. To avoid precipitation and/or aggregation, the recombinant [1–93]ApoA-I variants were neutralized by the addition of ammonium hydroxide, lyophilized, and stored at −70 °C until use. For experimental purposes, the variants were dissolved in 12 mM sodium phosphate buffer (pH 7.4), dialysed in the appropriate buffer, and centrifuged before use. Aliquots from each preparation were analysed by SDS-PAGE (15% polyacrylamide) and Western blotting using anti-human ApoA-I polyclonal antibodies (Dako, Denmark). Immunopositive signals were detected with a chemiluminescence system (West Pico, Pierce, Rockford, IL).

Mass spectrometry analysis

Recombinant wild-type [1–93]ApoA-I and all its mutational mutants studied in the present work were analysed by MS. Aliquots of peptide samples were dissolved in 12 mM phosphate buffer at pH 7.4 and desalted by HPLC on a HP 1100 (Agilent Technologies; Santa Clara, CA) by using a Phenomenex narrow-bore C4 reverse-phase column (250 × 32 mm) with 0.1% TFA (solvent A) and 0.07% TFA in 95% acetonitrile (solvent B). The samples were eluted by means of a linear gradient from 20% to 95% of solvent B over a course of 10 min. HPLC fractions were manually collected and introduced into the electrospray ion source of a QUATTRO MICRO mass spectrometer (Waters, Milford, MA) by direct injection. Full-scan MS spectra were acquired in a 700–1400 m/z range at 10 s per scan. Calibration was achieved by injecting separately a protein of known mass (heart horse myoglobin, 16,951.5 Da); all values are reported as average masses. The same procedure has been applied for the analysis of nonoxidised and fully oxidised wild-type and variant L75P [1–93]ApoA-I. The peptides were oxidised by incubation with 0.3% hydrogen peroxide in 100 mM sodium phosphate (pH 7.4) at 37 °C for 8 h as reported by Wong *et al.*[27]

Gel-filtration chromatography

Gel-filtration experiments were performed with a SMART system (Pharmacia Biotech) using a Superdex-75 column (Pharmacia) equilibrated and eluted in 50 mM phosphate buffer (pH 7.5) containing 150 mM NaCl. [1–93]ApoA-I (4 μg) was dissolved in an appropriate volume of buffer to a final concentration of 7 μM. Experiments were performed at room temperature at a flow rate of 75 μl/min. The column was calibrated under the same conditions with standard proteins.

Analytical equilibrium ultracentrifugation

Sedimentation equilibrium analysis was performed at 20 °C in a Beckman XL-I ultracentrifuge with an An-50 Ti rotor (Beckman-Coulter UK Ltd., Bucks, UK), and absorbance was monitored at 280 nm. Wild-type [1–93] ApoA-I was dissolved at 0.1, 0.2, and 0.3 mg/ml in 50 mM sodium phosphate (pH 7.5) containing 150 mM NaCl, and 100 μl of each sample was analyzed using six-sector cells with a column height of 2 mm and a rotor speed of 42,000 rpm. Data were fitted using Beckman software provided as an add-on to Origin version 4.1 (MicroCal, GE Healthcare), where the partial specific volume was 0.7298 mL/g and buffer density and viscosity were calculated according to the SEDNTERP program.

Circular dichroism

Circular dichroism spectra were recorded on a Jasco J-710 spectropolarimeter as previously described.[13] Measurements were performed at 20 °C at a protein concentration of 0.2 mg/ml in 3 mM glycine, 3 mM sodium acetate, and 3 mM sodium phosphate at pH 7 (buffer A). Acidification of the solutions was carried out as previously described,[13] and CD data were expressed as mean residue ellipticity (θ). The α-helical content of the samples was assessed using the K2D2 software, which is available online§.[10]

Light scattering

The level of overall aggregation was determined by measurement of solution turbidity at 350 nm using a Jasco W-650 spectrophotometer. Samples of each variant of [1–93]ApoA-I at a final concentration of 0.3 mg/ml in 3 mM glycine, 3 mM sodium acetate, and 3 mM sodium phosphate at pH 4 were incubated at 4 °C. The process of aggregation was monitored spectrophotometrically throughout the experiment. Experimental data were fitted to single exponential functions to determine the aggregation rate constants (k_{AGG}), and a statistical analysis was performed using Fisher's least significant difference test with the STATGRAPHICS Plus software.

Fourier transform infrared spectroscopy

[1–93]ApoA-I variants were incubated at 4 °C for 48 h at a concentration of 0.3 mg/ml in a solution of 3 mM sodium phosphate, 3 mM sodium acetate at pH 4. The aggregated material, collected after centrifugation and rinsed in water/HCl at pH 4, was deposited on a single reflection diamond element of an attenuated total reflection (ATR) device (Golden Gate, Specac, UK). After solvent evaporation, ATR/FTIR spectra were collected using a FTS40A spectrometer (Bio-Rad, Digilab Division, Cambridge, MA, USA), equipped with a nitrogen-cooled mercury-cadmium-tellurium detector (narrow band, 250 μm), under the following conditions: 2 cm^{-1} spectral resolution, 20 kHz scan speed, 1000 scan co-addition, and triangular apodization. Before computing the second

§http://www.ogic.ca/projects/k2d2/–>http://www.ogic.ca/projects/k2d2/

derivative of the spectra, a binomial smoothing (11 points) of the measured data was applied. The second derivative of the spectrum was then performed following the Savitsky–Golay method with the Grams 32 software (Galactic Industries Corporation, USA), using a 3rd polynomial order and 5 interpolated points.

To evaluate the proportion of β-sheet structures in the aggregates of the different [1–93]ApoA-I variants, we performed a curve fitting of the amide I band in the measured spectra as a linear combination of Gaussian components, following a previously described approach.[28,29] The number of Gaussian functions and their peak positions were taken from second-derivative and Fourier self-deconvoluted spectra. In a first step, we kept fixed peak positions and let the other parameters to be adjusted iteratively. In a second step, all the fitting parameters were allowed to change in order to obtain the set of best-fitting Gaussian components. Their fractional area represents the percentage of the corresponding secondary structure. This analysis was performed using the Grams 32 software (Galactic Industries Corporation, USA).

Atomic force microscopy

[1–93]ApoA-I variants were incubated at 4 °C for 48 h at a concentration of 0.4 mg/ml in 10 mM sodium phosphate (pH 4). For the AFM study, 10-μl aliquots were deposited on freshly cleaved mica and dried under mild vacuum. Before deposition on mica, each sample was diluted 50 times using Milli-Q water to avoid the formation of salt crystals. Tapping-mode AFM measurements were performed in air using a Dimension 3100 scanning probe microscope equipped with a G-scanning head (maximum scan size, 100 μm) and driven by a Nanoscope IIIa controller and a Multimode scanning probe microscope equipped with an E scanning head (maximum scan size 10 μm) and driven by a Nanoscope IV controller (Digital Instruments, Veeco, Santa Barbara, CA, USA). Images were acquired in tapping mode in air using single-beam uncoated silicon cantilevers (type OMCL-AC160TS, Olympus, Tokyo, Japan). The drive frequency was typically 300 kHz, and the scan rate was between 0.5 and 2.0 Hz. Aggregate sizes were measured from the heights in cross-section of the topographic AFM images. As a consequence of sample dehydration, the measured aggregate heights are reduced with respect to those obtained under hydrated conditions; to obtain estimates of the latter ones, the heights reported in the results can be multiplied by a factor of about 2.2.[30]

Prediction of aggregation propensities

Aggregation propensity profiles at pH 4 of full-length ApoA-I, and [1–93]ApoA-I, and eight mutational variants were calculated using the Zyggregator method, which provides an estimate of the aggregation propensities of the different regions of a sequence on the basis of the physico-chemical properties of its amino acids.[6]

In the approach described in this paper, the intrinsic aggregation propensities of individual amino acids are defined as

$$p_i^{\mathrm{agg}} = \alpha_{\mathrm{h}} p_{\mathrm{h}} + \alpha_{\mathrm{s}} p_{\mathrm{s}} + \alpha_{\mathrm{hyd}} p_{\mathrm{hyd}} + \alpha_{\mathrm{c}} p_{\mathrm{c}} \quad (1)$$

where p_{h} and p_{s} are the propensities for α-helix and β-sheet formation of the amino acid at position i, and p_{hyd} and p_{c} are the hydrophobicity and charge, respectively. These propensities are then combined in a linear way with coefficients α determined as described below. The p_i^{agg} values are combined to provide a profile, A^p, which describes the intrinsic propensity for aggregation as a function of the complete amino acid sequence (Eq. 1). At each position i along the sequence, we define the profile A^p as an average over a window of seven residues

$$A_i^p = \frac{1}{7}\sum_{j=-3}^{3} p_{\mathrm{i+j}}^{\mathrm{agg}} + \alpha_{\mathrm{pat}} \mathrm{I}_{\mathrm{i}}^{\mathrm{pat}} + \alpha_{\mathrm{gk}} \mathrm{I}_{\mathrm{i}}^{\mathrm{gk}} \quad (2)$$

where I_i^{pat} is the term that takes into account the presence of specific patterns of alternating hydrophobic and hydrophilic residues (Eq. 1), and I_i^{gk} is the term that takes into account the gatekeeping effect of individual charges c_i

$$I_i^{\mathrm{gk}} = \sum_{j=-10}^{10} c_{i+j} \quad (3)$$

In order to compare the intrinsic propensity profiles, we normalize A^p by considering the average (μ_A) and the standard deviation (σ_A) at each position i for random sequences. We thus obtain the normalized intrinsic aggregation propensity profile

$$Z_i^p = \frac{A_i^p - \mu}{\sigma} \quad (4)$$

where we calculated the average μ and the standard deviation σ over random sequences

$$\mu = \frac{1}{(N-8)\cdot N_S}\sum_{k=1}^{N_S}\sum_{i=4}^{N-4} A_i^p(S_k)$$
$$\sigma^2 = \frac{1}{(N-8)\cdot N_S}\sum_{k=1}^{N_S}\sum_{i=4}^{N-4}\left(A_i^p(S_k) - m\right)^2 \quad (5)$$

Prediction of conformational fluctuations

The sequence-based predictions of the conformational fluctuations of wild-type [1–93]ApoA-I and the eight mutational variants considered in this work were carried out using the CamP method.[7] This method uses the physico-chemical properties of the amino acid sequences to estimate the local stabilities of the different regions of a folded state; the results are presented in the form of protection factors for hydrogen exchange.[7]

Supplementary materials related to this article can be found online at doi:10.1016/j.jmb.2011.01.044

Acknowledgements

We thank Silvia Torrassa and Amanda Penco for help with the AFM measurements. This work was partially supported by MIUR with the PRIN and

FIRB projects, Fondazione Cariplo, Ministero della Salute Progetto Strategico Malattie Rare, and Regione Lombardia.

References

1. Fielding, C. J. & Fielding, P. E. (1995). Molecular physiology of reverse cholesterol transport. *J. Lipid Res.* **36**, 211–228.
2. Sorci-Thomas, M. G. & Thomas, M. J. (2002). The effects of altered apolipoprotein A-I structure on plasma HDL concentration. *Trends Cardiovasc. Med.* **12**, 121–128.
3. Obici, L., Franceschini, G., Calabresi, L., Giorgetti, S., Stoppini, M., Merlini, G. & Bellotti, V. (2006). Structure, function and amyloidogenic propensity of apolipoprotein A-I. *Amyloid*, **13**, 191–205.
4. Mucchiano, G. I., Jonasson, L., Häggqvist, B., Einarsson, E. & Westermark, P. (2001). Apolipoprotein A-I-derived amyloid in atherosclerosis Its association with plasma levels of apolipoprotein A-I and cholesterol. *Am. J. Clin. Pathol.* **115**, 298–303.
5. Eriksson, M., Schönland, S., Yumlu, S., Hegenbart, U., von Hutten, H., Gioeva, Z. *et al.* (2009). Hereditary apolipoprotein AI-associated amyloidosis in surgical pathology specimens: identification of three novel mutations in the APOA1 gene. *J. Mol. Diagn.* **11**, 257–262.
6. Tartaglia, G. G., Pawar, A. P., Campioni, S., Dobson, C. M., Chiti, F. & Vendruscolo, M. (2008). Prediction of aggregation-prone regions in structured proteins. *J. Mol. Biol.* **380**, 425–436.
7. Tartaglia, G. G., Cavalli, A. & Vendruscolo, M. (2007). Prediction of local structural stabilities of proteins from their amino acid sequences. *Structure*, **15**, 139–143.
8. Obici, L., Bellotti, V., Mangione, P., Stoppini, M., Arbustini, E., Verga, L. *et al.* (1999). The new apolipoprotein A-I variant Leu(174)→Ser causes hereditary cardiac amyloidosis, and the amyloid fibrils are constituted by the 93-residue N-terminal polypeptide. *Am. J. Pathol.* **155**, 695–702.
9. Di Gaetano, S., Guglielmi, F., Arciello, A., Mangione, P., Monti, M., Pagnozzi, D. *et al.* (2006). Recombinant amyloidogenic domain of ApoA-I: analysis of its fibrillogenic potential. *Biochem. Biophys. Res. Commun.* **351**, 223–228.
10. Perez-Iratxeta, C. & Andrade-Navarro, M. A. (2008). K2D2: estimatation of protein secondary structure from circular dichroism spectra. *BMC Struct. Biol.* **8**, 25.
11. Seshadri, S., Khurana, R. & Fink, A. L. (1999). Fourier transform infrared spectroscopy in analysis of protein deposits. *Methods Enzymol*, **309**, 559–576.
12. Natalello, A., Prokorov, V. V., Tagliavini, F., Morbin, M., Forloni, G., Beeg, M. *et al.* (2008). Conformational plasticity of the Gerstmann–Sträussler–Scheinker disease peptide as indicated by Its multiple aggregation pathways. *J. Mol. Biol.* **381**, 1349–1361.
13. Andreola, A., Bellotti, V., Giorgetti, S., Mangione, P., Obici, L., Stoppini, M. *et al.* (2003). Conformational switching and fibrillogenesis in the amyloidogenic fragment of apolipoprotein A-I. *J. Biol. Chem.* **278**, 2444–2451.
14. Arrondo, J. L. R. & Goni, F. M. (1999). Structure and dynamics of membrane proteins as studied by infrared spectroscopy. *Prog. Biophys. Mol. Biol.* **72**, 367–405.
15. Scalvini, T., Martini, P. R., Obici, L., Tardanico, R., Biasi, L., Gregorini, G. *et al.* (2007). Infertility and hypergonadotropic hypogonadism as first evidence of hereditary apolipoprotein A-I amyloidosis. *J. Urol.* **178**, 344–348.
16. Monti, D. M., Guglielmi, F., Monti, M., Cozzolino, F., Torrassa, S., Relini, A. *et al.* (2010). Effects of a lipid environment on the fibrillogenic pathway of the N-terminal polypeptide of human apolipoprotein A-I, responsible for *in vivo* amyloid fibril formation. *Eur. Biophys J.* **39**, 1289–1299.
17. Lagerstedt, J. O., Budamagunta, M. S., Oda, M. N. & Voss, J. C. (2007). Electron paramagnetic resonance spectroscopy of site-directed spin labels reveals the structural heterogeneity in the N-terminal domain of apoA-I in solution. *J. Biol. Chem.* **282**, 9143–9149.
18. Ajees, A. A., Anantharamaiah, G. M., Mishra, V. K., Hussain, M. M. & Murthy, H. M. (2006). Crystal structure of human apolipoprotein A-I: insights into its protective effect against cardiovascular diseases. *Proc. Natl Acad. Sci. USA*, **103**, 2126–2131.
19. Lagerstedt, J. O., Cavigiolio, G., Roberts, L. M., Hong, H. S., Jin, L. W., Fitzgerald, P. G. *et al.* (2007). Mapping the structural transition in an amyloidogenic apolipoprotein A-I. *Biochemistry*, **46**, 9693–9699.
20. Nichols, W. C., Dwulet, F. E., Liepnieks, J. & Benson, M. D. (1988). Variant apolipoprotein AI as a major constituent of a human hereditary amyloid. *Biochem. Biophys. Res. Commun.* **156**, 762–768.
21. Soutar, A. K., Hawkins, P. N., Vigushin, D. M., Tennent, G. A., Booth, S. E., Hutton, T. *et al.* (1992). Apolipoprotein AI mutation Arg-60 causes autosomal dominant amyloidosis. *Proc. Natl Acad. Sci. USA*, **89**, 7389–7393.
22. Booth, D. R., Tan, S. Y., Booth, S. E., Hsuan, J. J., Totty, N. F., Nguyen, O. *et al.* (1995). A new apolipoprotein Al variant, Trp50Arg, causes hereditary amyloidosis. *Q.J.M.* **88**, 695–702.
23. Booth, D. R., Tan, S. Y., Booth, S. E., Tennent, G. A., Hutchinson, W. L., Hsuan, J. J. *et al.* (1996). Hereditary hepatic and systemic amyloidosis caused by a new deletion/insertion mutation in the apolipoprotein AI gene. *J. Clin. Invest.* **97**, 2714–2721.
24. Persey, M. R., Booth, D. R., Booth, S. E., van Zyl-Smit, R., Adams, B. K., Fattaar, A. B. *et al.* (1998). Hereditary nephropathic systemic amyloidosis caused by a novel variant apolipoprotein A-I. *Kidney Int.* **53**, 276–281.
25. Murphy, C. L., Wang, S., Weaver, K., Gertz, M. A., Weiss, D. T. & Solomon, A. (2004). Renal apolipoprotein A-I amyloidosis associated with a novel mutant Leu64Pro. *Am. J. Kidney Dis.* **44**, 1103–1109.
26. Aiyar, A., Xiang, Y. & Leis, J. (1996). Site-directed mutagenesis using overlap extension PCR. *J. Methods Mol. Biol.* **57**, 177–191.
27. Wong, Y. Q., Binger, K. J., Howlett, G. J. & Griffin, M. D. (2010). Methionine oxidation induces amyloid fibril formation by full-length apolipoprotein A-I. *Proc. Natl Acad. Sci. USA*, **107**, 1977–1982.
28. Natalello, A., Ami, D., Brocca, S., Lotti, M. & Doglia, S. M. (2005). Secondary structure, conformational stability and glycosylation of a recombinant Candida rugosa lipase studied by Fourier-transform infrared spectroscopy. *Biochem. J.* **385**, 511–517.

29. Vila, R., Ponte, I., Collado, M., Arrondo, J. L. & Suau, P. (2001). Induction of secondary structure in a COOH-terminal peptide of histone H1 by interaction with the DNA: an infrared spectroscopy study. *J. Biol. Chem.* **276**, 30898–30903.

30. Campioni, S., Mannini, B., Zampagni, M., Pensalfini, A., Parrini, C., Evangelisti, E. *et al.* (2010). A causative link between the structure of aberrant protein oligomers and their toxicity. *Nature Chem. Biol.* **6**, 140–147.